

Supplementary

Synergistic Effect of Heterostructured Dissimilar Metal-Organic Framework Thin Films on Adsorption Properties.

Zheng Wang,^{a,b} Suttipong Wannapaiboon,^c Sebastian Henke,^d Michael Paulus,^e Katia Rodewald,^f
Bernhard Rieger,^f Roland A. Fischer^{*a}

^aChair of Inorganic and Metal-Organic Chemistry, Department Chemistry & Catalysis Research Center, Technical University of Munich (TUM), Lichtenbergstr. 4, 85748 Garching, Germany

^bCollege of Food Science and Engineering, Northwest University, 710069 Xi'an, Shaanxi, China.

^cSynchrotron Light Research Institute (SLRI), 111 University Avenue, Muang District, 30000 Nakhon Ratchasima, Thailand

^dAnorganische Chemie, Fakultät für Chemie und Chemische Biologie, Technische Universität Dortmund, Otto-Hahn Str. 6, 44227 Dortmund, Germany

^eFakultät Physik/DELTA, Technische Universität Dortmund, Maria-Goeppert-Mayer-Str. 2, 44221 Dortmund, Germany

^fWACKER-Chair of Macromolecular Chemistry, Department Chemistry & Catalysis Research Center, Technical University of Munich (TUM), Lichtenbergstr. 4, 85748 Garching, Germany

Experimental Details and Characterization

Materials

All chemicals are commercially available and were used as received without further purification.

General methods

The crystallinity and orientation of obtained SURMOFs were identified by grazing incidence X-ray diffraction (GIXRD, Panalytical Empyrean instrument, grazing incidence mode, room temperature, Cu-K α radiation, the range of $2\theta = 5\text{--}18^\circ$, a step size of 0.01313° , accumulation time 1.5s per step) and two dimensional-GIXRD (2D-GIXRD, Beamline 9 DELTA Synchrotron, Dortmund, at room temperature with monochromatic X-rays with a wavelength of 0.9607 \AA , MAR345 detector, the sample-to-detector distance was 354.37 mm). Infrared reflection absorption spectroscopy (IRRAS) measurements were done on a Biorad Excalibur FTIR spectrometer (FTS 3000) with 2 cm^{-1} resolution at an angle of incidence of 80° relative to the surface normal and further processed by using boxcar apodization. Scanning electron microscopy (SEM) images were taken by a JEOL JSM-7500F Field Emission Scanning Electron Microscope under Gentle Beam mode. VOCs (methanol, benzene, cyclohexane and mesitylene) adsorption isotherms of the SURMOFs were measured by an environmental-controlled quartz crystal microbalance (BEL-QCM instrument, BEL Japan). Prior to the sorption measurements, the SURMOFs were activated by soaking in pure CH_2Cl_2 for 2 days at room temperature and subsequently dried in a pure N_2 stream. Subsequently, the samples were placed in the BEL-QCM instrument cells at 25°C in a He stream (99.999%, 100 sccm) for about 4 hours. After the activation process, the QCM frequency was recorded when the frequency change was stable within $\pm 5 \text{ Hz}$ over 30 min. Afterwards, VOCs sorption isotherms were collected by varying the relative vapor pressure (P/P_0) of saturated vapor of probe molecules in a He gas stream at 25°C ranging from 0 to 95.0%. The mass of the SURMOFs and adsorption amounts were calculated from the difference of the read QCM frequency and the fundamental frequency of the bare QCM substrate according to Sauerbrey's equation.

Thin film growth

Herein, the Au-coated QCM substrates (AT cut type, Au electrode, diameter 14 mm, thickness 0.3 mm, and fundamental frequency ca. 4.95 MHz) were used for thin film growth. Prior to the film growth, QCM substrates were cleaned by immersing in the solution of water/ H_2O_2 /ammonia with volume ratio of 5 : 1 : 1 at 75°C for 15 min. After, the cleaned QCM substrates were functionalized by soaking in a $20 \mu\text{M}$ SAM solution of 16-mercaptohexadecanoic acid (MHDA) in ethanol for one day under room temperature followed by rinsing with pure ethanol.

In this work, all of SURMOFs were fabricated by stepwise LPE for certain cycles using the automated QCM instrument Q-Sense E4 Auto at 40 °C with a flow rate of 100 μ L/min. In each deposition cycle, the functionalized QCM substrate was first exposed to 0.5 mM $\text{Cu}(\text{OAc})_2 \cdot \text{H}_2\text{O}$ ethanol solution for 5 min and then 0.2 mM linker (H_2bdc or H_3btc) ethanol solution for 10 min. Each subsequent step of dosing components was separated by a washing step with absolute ethanol for 5 min. After repeating this procedure for a certain number of cycles, the SURMOF with specific thickness can be obtained. Note that, the solution of linker was prepared using mixed solvent of water and ethanol (5% H_2O for H_2bdc and 20% H_2O for H_3btc). As a typical example, hetero-SURMOF $\text{Cu}_3\text{btc}_2(40)\text{-on-Cubdc}(40)$ (**B(40)-on-1(40)**) was fabricated by firstly dosing 40 cycles $\text{Cu}(\text{OAc})_2/\text{H}_3\text{btc}$ and then followed by dosing 40 cycles $\text{Cu}(\text{OAc})_2/\text{H}_2\text{bdc}$.

The frequency change of QCM sensor against time curve is shown in Figure S1 (only hetero-SURMOF **B-on-A1** is presented for clarity), from which it is clear to distinguish the growth region of SURMOF **A1** (40 cycles) and **B** (40 cycles). The hetero-SURMOF with reversed order **A1-on-B** was also fabricated by the same method, the frequency change-time curve, XRD and methanol sorption isotherm are presented in Figure S2. We would not put more attention on **A1-on-B** because of its mediocre sorption property.

Crystallinity of SURMOFs

The crystallinity and crystallographic orientation of obtained homo- and hetero-SURMOFs were checked by GIXRD and 2D-GIXRD. The XRD patterns of homo-SURMOF **A** (general term of **A1**, Cu_2bpdcc (**A2**, bpdcc = biphenyl-4,4'-dicarboxylate) and CuTF-bdc (**A3**, TF-bdc = tetrafluoroterephthalate)) and **B** are shown in Figure S3a, and they correspond to the calculated or reported ones. As also can be seen in Figure S3b, reflections of both SURMOF **A** and **B** are present in the XRD patterns of hetero-SURMOFs, which attests the presence of both phases in heterostructures. The successful growth of MOF **B** on the top of SURMOF **A** could be ascribed to the structural flexibility of 2D SURMOF **A**, which provides the tolerance for bridging the mis-matched lattices of both frameworks. Interestingly, by analyzing XRD patterns we found that the crystallographic orientation of upper MOF **B** is determined by the linkers used in bottom SURMOF **A** despite it solely orients along the (100) direction. Specifically, MOF **B** mainly shows the orientation of (100) on SURMOF **A1**, while it has no preferred orientation on SURMOFs **A2** and **A3**. Note that the pre-formed SURMOFs **A** (fabricated with 5% water in linker solution) are quite stable and will not be affected by the component solutions of MOF **B** (with 20% water in linker solution) according to the literature.¹

Furthermore, 2D-GIXRD measurements were also performed using synchrotron

radiation to confirm the presence of both phases, MOF **A** and **B**. The one-dimensional (1D) GIXRD profiles were extracted from the original 2D images of hetero-SURMOF **B-on-A** along different angles shown in Figure S4. The in-plane XRD patterns (along with 0 or 180°) are shown in Figure S5, from which both peaks from MOF **A** and **B** are observed. Specifically, all of the SURMOF **A** and MOF **B** reflections are corresponding to the calculated or reported ones.²

IRRAS

The IRRAS spectra were recorded to verify the presence of SURMOF **A** and **B** in obtained heterostructures, which are presented in Figure S8. By analyzing these spectra, there is no doubt that both signals of SURMOF **A** and **B** are found in heterostructures which proves the successful synthesis of hetero-SURMOF **B-on-A**.

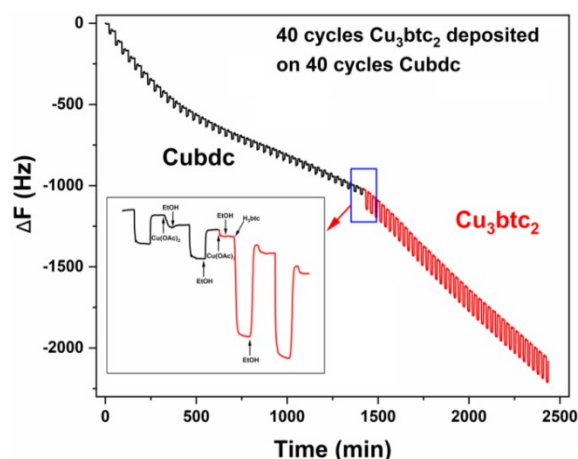


Figure S1. The changes in the QCM oscillator frequency (ΔF) as a function of time during the stepwise LPE growth process of hetero-SURMOF **B-on-A1**, from which it is easy to know that the relative frequency change or mass ratio **A1** and **B** is about 1:1.

According to the changes in the QCM oscillator frequency (ΔF) as a function of time during the stepwise LPE growth process of hetero-SURMOF **B(40)-on-A1(40)**, we converted the total storage capacity/adsorption ability based on per unit mass of MOF to the values based on per unit molar of total MOF. Herein, we performed mathematical calculations on **B-on-A1** as an example, and the calculation process of **B-on-A2** and **B-on-A2** are the same.

Table S1. The calculation of total moles of 1g hetero-SURMOF.

SURMOFs	Chemical formula	FW (g/mol)	Norm. mass SURMOF (g)	Total moles (mmol) of 1 g SURMOF
Cubdc	$\text{CuC}_8\text{H}_4\text{O}_4$	227.66	1	4.393
$\text{Cu}_3(\text{btc})_2$	$\text{Cu}_3\text{C}_{18}\text{H}_6\text{O}_{12}$	604.87	1	1.653
B(40)-on-A1(40) 50% w/w $\text{Cu}_3(\text{btc})_2$ + 50% w/w Cubdc (ΔF of QCM monitoring)	$\text{Cu}_3\text{C}_{18}\text{H}_6\text{O}_{12}$ $\text{CuC}_8\text{H}_4\text{O}_4$	604.87 227.66	Total 1 g 0.5 0.5	Total 3.203 mmol 0.827 2.196

Table S2. The conversion of values from based on per unit mass of MOF to that based on per unit molar of total MOF.

Adsorbate	B(40) (1 g \rightarrow 1.653 mmol)		B(40)-on-A1(40) (1g \rightarrow 3.203 mmol)	
	mmol VOC / g SURMOF	mol VOC / mol SURMOF	mmol VOC / g SURMOF	mol VOC / mol SURMOF
Methanol	11.39 (1)	6.89 (1)	10.25 (0.90)	3.20 (0.46)
Benzene	3.77 (1)	2.28 (1)	4.32 (1.15)	1.35 (0.59)
Cyclohexane	1.17 (1)	0.71 (1)	2.69 (2.30)	0.84 (1.18)
Mesitylene	0.99 (1)	0.60 (1)	2.41 (2.43)	0.75 (1.25)

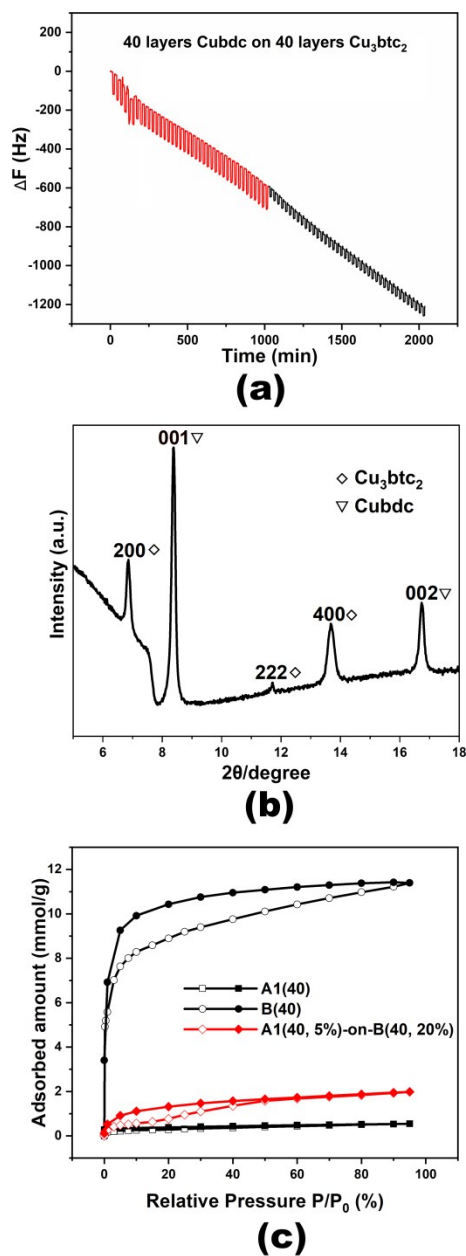


Figure S2. (a) The QCM frequency changes against time curve of stepwise LPE growth process of hetero-SURMOF **A1-on-B**; (b) XRD pattern of hetero-SURMOF **A1-on-B**; (c) the methanol sorption isotherms of hetero-SURMOF **A1-on-B** and the homo-SURMOF **A1** and **B**. Note that, the hollow shapes are adsorption and solid ones are desorption.

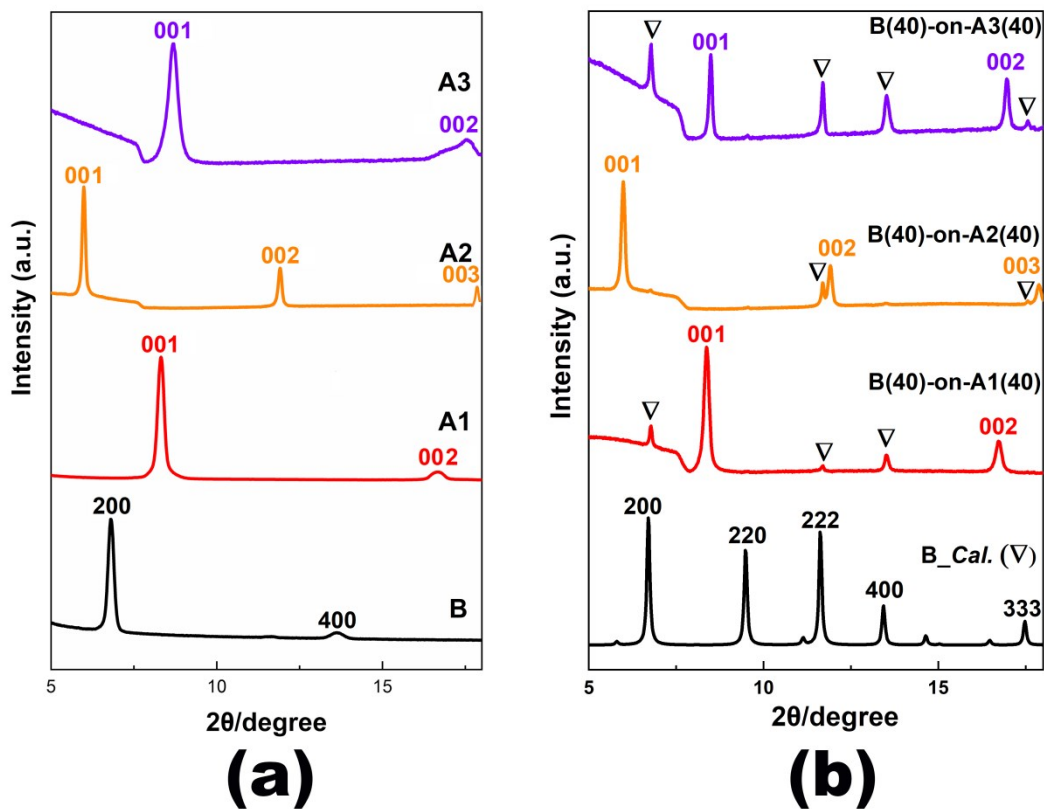


Figure S3. The XRD patterns of (a) homo-SURMOF **B**, **A1**, **A2** and **A3**, and (b) hetero-SURMOF **B-on-A1/A2/A3**. Triangles are the peaks of MOF **B** and the circles are from SURMOF **A**. Note that the indices of the reflections of SURMOF **A1** and its isorecticular analogues **A2** and **A3** were matched with the non-conventional crystallographic setting of the tetragonal cell used by H. K. Arslan et al (ref 42) and J. Liu et al (SI ref 2). In these reports, the authors used the crystallographic *b* axis as the unique (i.e. fourfold symmetric) axis instead of the conventional *c* axis. We use this non-conventional setting throughout the manuscript.

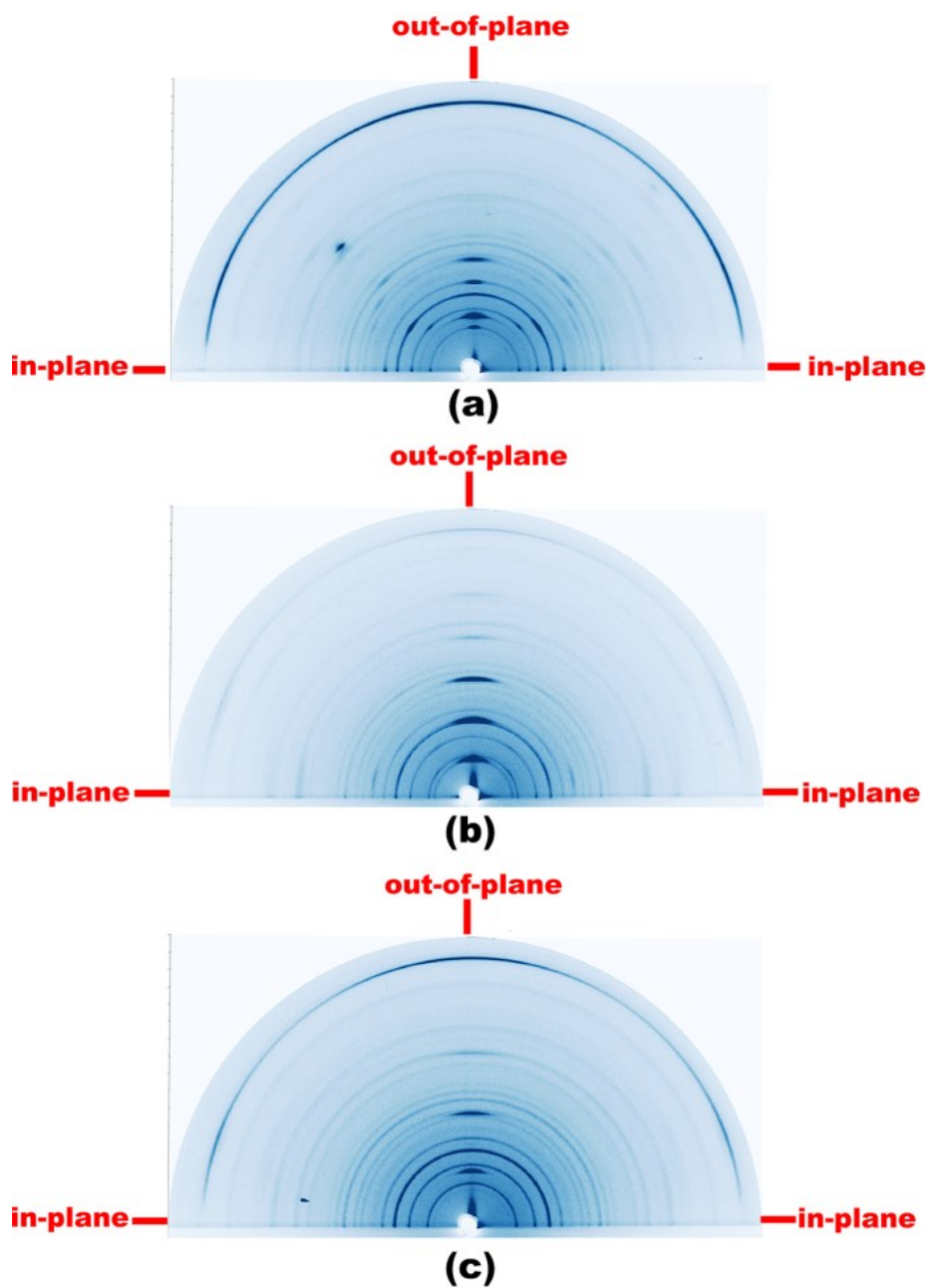


Figure S4. The 2D-GIXRD images of hetero-SURMOFs (a) **B-on-A1**, (b) **B-on-A2**, (c) **B-on-A3** collected at DELTA, Dortmund at room temperature with a monochromatic X-ray beam with a photon wavelength of 0.9607 Å. As marked in the figure, the horizontal (90°) and vertical direction (0 or 180°) are in-plane and out-of-plane pattern, respectively.

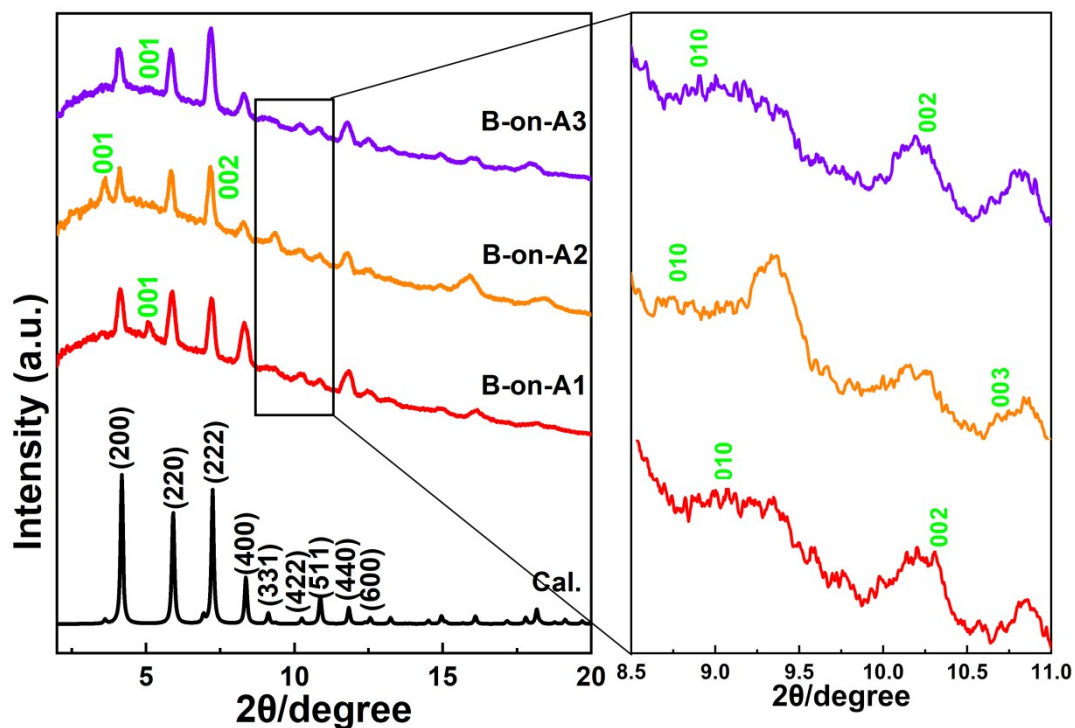


Figure S5. The in-plane XRD patterns of hetero-SURMOF **B-on-A1** (red), **B-on-A2** (orange) and **B-on-A3** (violet) extracted from the original 2D-GIXRD images. The green and black indices of reflections are from MOF **A** and **B**, respectively. Note that, the 2D-GIXRD measurements were performed with a monochromatic X-ray beam with a wavelength of 0.9607 Å. The simulated pattern of MOF **B** was calculated with the program Mercury by setting the wavelength to 0.9607 Å.

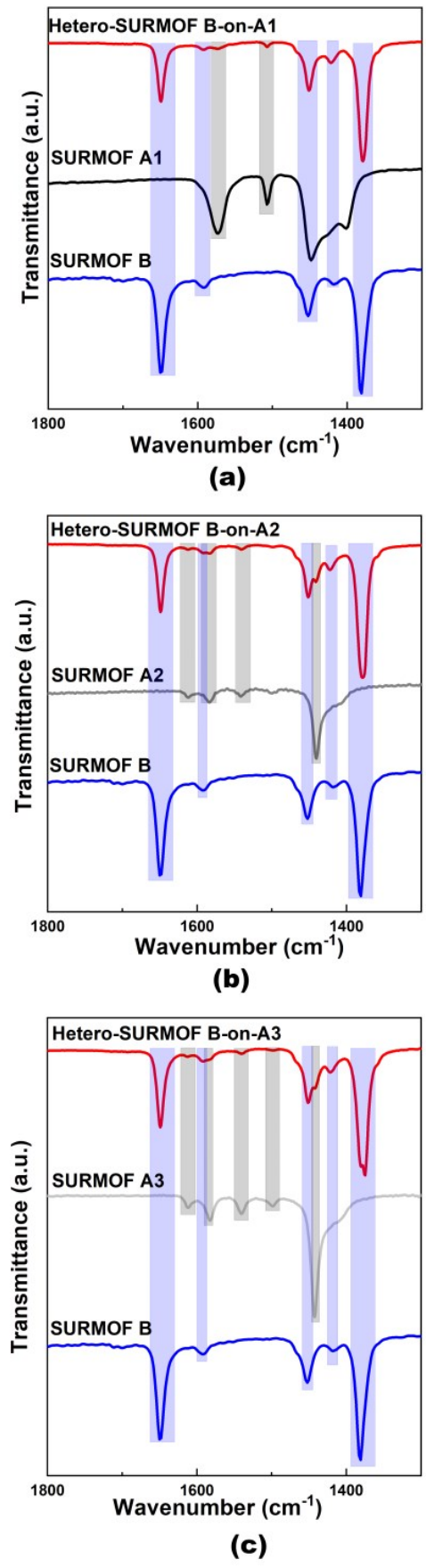


Figure S6. The IRRAS spectra of hetero-SURMOF (a) **B-on-A1**; (b) **B-on-A2**; (c) **B-on-A3**.

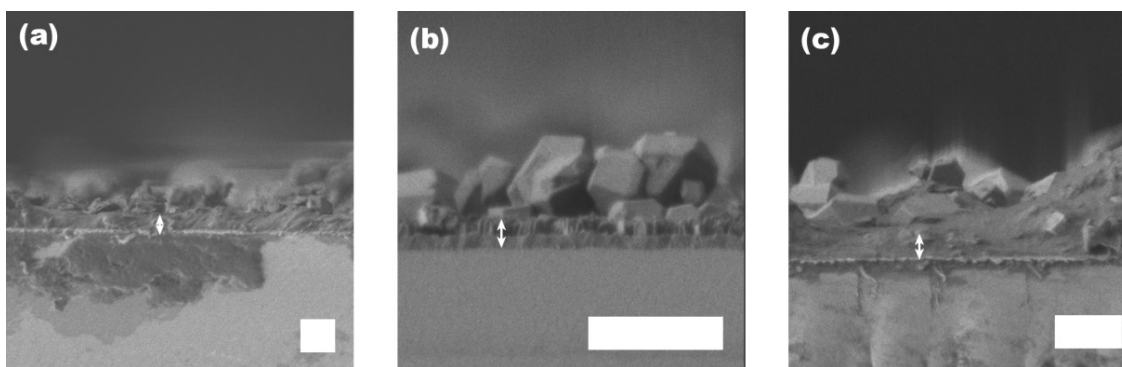


Figure S7. The cross-section SEM images of (a) hetero-SURMOF **B-on-A1**; (b) hetero-SURMOF **B-on-A2**; and (c) hetero-SURMOF **B-on-A1**. Note that, the scale bar is 1 μm . From the figures we can estimate the thickness of hetero-SURMOFs around 350, 230 and 390 nm, respectively.

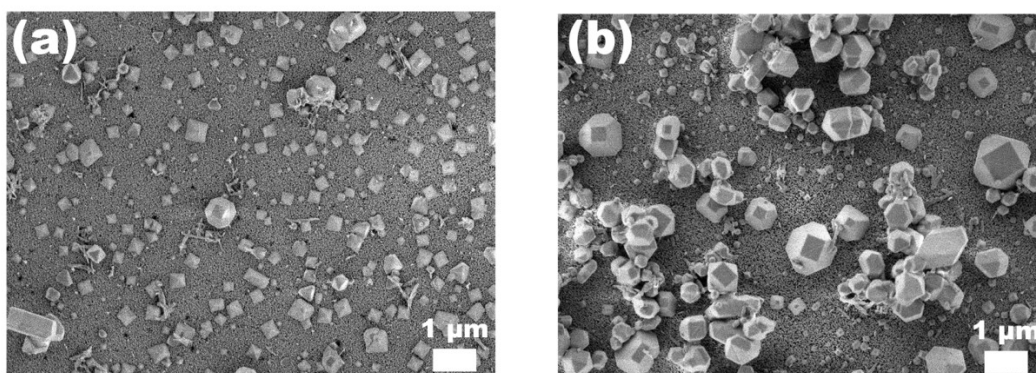


Figure S8. The morphology of (a) hetero-SURMOF **B(20, 20%)**-on-**A1(40, 5%)**, and (b) **B(40, 20%)**-on-**A1(40, 5%)**. Herein, the **B(20, 20%)** means that 20 cycles MOF **B** fabricated integrating 20% additional water in linker H_3btc solution, and the rest are the same. With depositing more MOF **B** on SURMOF **A1**, the interfacial area between the two MOF types is increased.

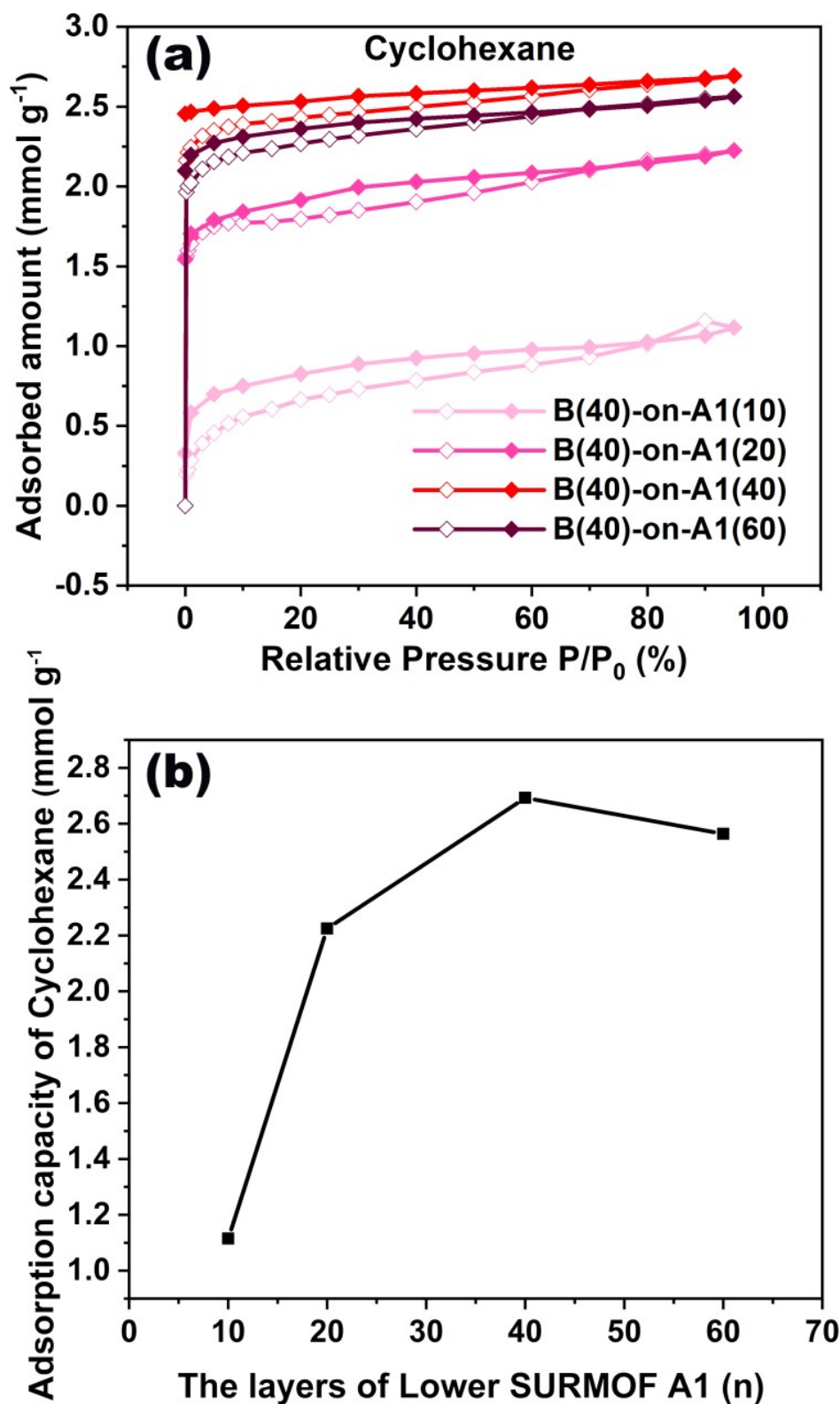


Figure S9. (a) The cyclohexane sorption isotherms of hetero-SURMOF **B-on-A1** with 40 cycles SURMOF **B** on the top of 10, 20, 40 and 60 cycles of SURMOF **A1**; (b) the comparison of the cyclohexane adsorption capacity of hetero-SURMOFs **B(40)-on-A(10/20/40/60)**.

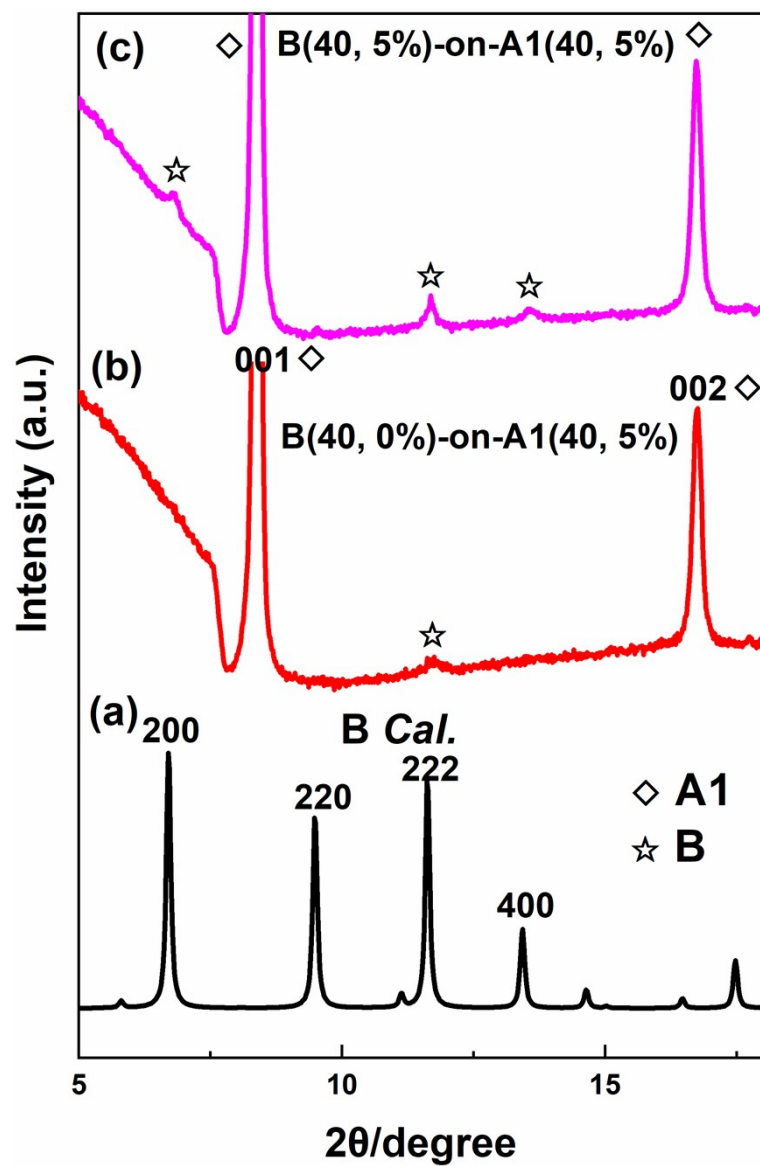


Figure S10. The XRD patterns of (a) calculated MOF B, (b) hetero-SURMOF B(0%)-on-A1(5%) and (c) hetero-SURMOF B(5%)-on-A1(5%).

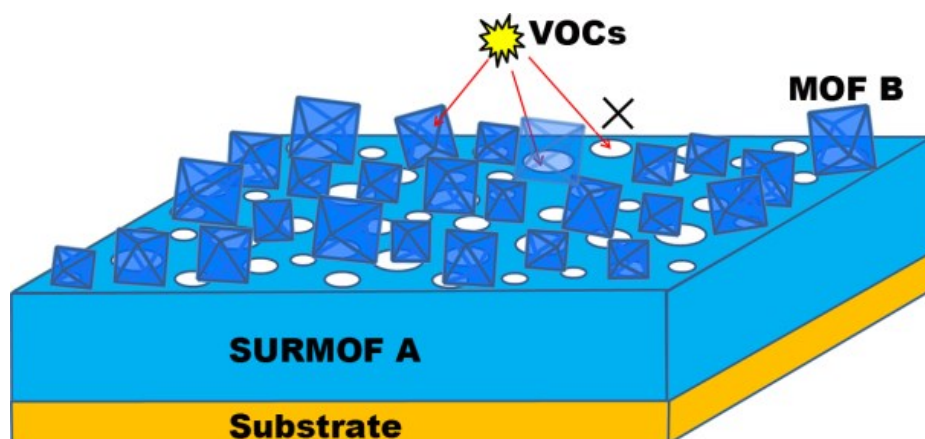


Figure S11. Schematic illustration of the formation of extrinsic porosity at the **A-B** interface. Considering the voids presented in SURMOF **A** thin films, the extrinsic interfacial porosity could be formed by the cover of MOF **B** crystals. In order to show the extrinsic porosity clear, one of MOF **B** crystal was drawn in lighter color than others.

Supplementary References

1. M. Hanke, H. K. Arslan, S. Bauer, O. Zybaylo, C. Christophis, H. Gliemann, A. Rosenhahn and C. Wöll, *Langmuir*, 2012, **28**, 6877.
2. J. Liu, B. Lukose, O. Shekhah, H. K. Arslan, P. Weidler, H. Gliemann, S. Brase, S. Grosjean, A. Godt, X. Feng, K. Mullen, I. B. Magdau, T. Heine and C. Wöll, *Sci. Rep.*, 2012, **2**, 921.